communications materials

A Nature Portfolio journal

Article

https://doi.org/10.1038/s43246-025-01040-6

# Coumarin-inspired light-responsive thermoplastic adhesives for recyclable multilayer packaging



Carlos Sedano [1], Manuel Herrero[2], Miriam Trigo-López [1], Miguel Angel Rodríguez-Pérez[2], Juan Carlos Merino[3], José Miguel García [1], Saul Vallejos [1] ✉ & Karina C. Núñez Carrero [2] ✉

Multilayer plastic packaging offers essential barrier and mechanical properties for food preservation, but its complex structure prevents effective recycling. Here, we report a light-responsive thermoplastic adhesive designed to enable on-demand separation of polymer layers in multilayer packaging. The adhesive adopts a triblock architecture with terminal blocks compatible with polyethylene (PE) and polyamide (PA), and a central segment functionalised with coumarin-based photoremovable groups. Upon ultraviolet (UV) exposure, the adhesive undergoes complete molecular breakdown, triggering clean delamination without solvents or mechanical force. Fabricated PE – photosensitive adhesive – PA films demonstrated superior adhesion performance compared to a commercial benchmark during service life, and efficient separation upon irradiation, as confirmed by Fourier transform infrared (FTIR) spectroscopy, microscopy, and T-peel testing. Life cycle assessment revealed that, while the laboratory-scale synthesis has higher environmental costs, the impact is offset after a single reuse cycle in projected industrial conditions, reaching up to 80% reduction after six cycles. This approach provides a scalable strategy to reconcile performance and recyclability in multilayer packaging.

Polymer-based packaging materials must reconcile demanding performance with ever-stricter environmental expectations, a tension that is particularly acute for multi-material, multilayer plastic packaging (MMPP) used in single-use food applications[1]. Roughly 40 % of global polymer production is devoted to packaging, and one-fifth of that total already ends up in MMPP structures[2]. These films, typically assembled from polyolefins, polyesters, polyamides, polyurethanes, and vinyl polymers, marry complementary properties—mechanical strength, sealability, barrier performance and even antimicrobial activity—by means of lamination or co-extrusion, with adhesive tie-layers ensuring cohesion[3]. Commercial food pouches and lidding films may contain three to eleven layers (seven is the industrial workhorse) compressed into less than 100 µm thickness; their low mass-per-area and complex architecture hinder collection, sorting, and mechanical recycling[4]. These thin, low-mass laminates also lack a credible monomaterial substitute that can deliver comparable barrier and seal performance under current industrial constraints, which further compounds end-of-life management challenges in high-volume food applications.

Because of this complexity, MMPP is now a major contributor to the growing stock of non-recyclable packaging waste, and the resulting environmental burden feeds a negative consumer perception. That judgement rarely recognises the resource savings delivered by modern packaging: it protects products whose manufacture consumes water, land and energy, prevents contamination, extends shelf-life and streamlines logistics, while simultaneously acting as an information and marketing platform[4–6]. Yet no industrially viable route exists to recycle the post-consumer and post-industrial fraction of these laminates—indeed, as much as 40 % of multilayer film produced never reaches the final pack because of trimming and converting losses—undermining progress towards a circular economy. In practice, therefore, any route to circularity for MMPP must directly address post-use layer separation without sacrificing in-service performance or imposing prohibitive processing penalties.

Adhesives sit at the heart of this dilemma. State-of-the-art systems — polyurethane, acrylic or maleated polyolefin formulations — secure excellent interfacial strength but make post-use disassembly extraordinarily difficult. The canonical example is a PE–adhesive–PA trilayer bonded with

[1]Departamento de Química, Facultad de Ciencias, Universidad de Burgos, Burgos, Spain. [2]Departamento de Física de la Materia Condensada, Cellmat Laboratory, Facultad de Ciencias, Universidad de Valladolid, Valladolid, Spain. [3]Departamento de Física de la Materia Condensada, Escuela de Ingenieros Industriales, Universidad de Valladolid, Valladolid, Spain. ✉e-mail: svallejos@ubu.es; karinacarla.nunez@uva.es

maleated polyethylene (PE-g-MA); condensation of anhydride and amide groups generates irreversible covalent linkages[7] (See Fig. 1a). Research, therefore, focuses on delamination methods, either dissolving or chemically degrading the tie-layer. Solvent approaches, guided by polymer-solution thermodynamics, can in principle recover clean fractions but raise their own environmental concerns[8–10]. Dynamic covalent adhesives based on Diels–Alder chemistry have been explored, yet high cost, processing constraints and limited performance keep most solutions at laboratory scale [11–13]; incineration remains the dominant fate of MMPP. However, solvent-based delamination raises its own environmental and operational burdens (solvent recovery, emissions, and quality loss), while dynamic covalent tie-layers explored to date typically rely on thermoset networks with limited compatibility with standard thermoplastic lamination lines and food-contact specifications. This leaves a clear technology gap for melt-processable, trigger-responsive adhesives that behave like conventional ties in service yet enable clean, on-demand disassembly at end-of-life.

Here, we introduce a photosensitive, fully thermoplastic adhesive that uses light to trigger physicochemical change. The design exploits coumarin chromophores—renowned photoremovable protecting groups that, upon UV irradiation, undergo heterolytic cleavage to release a coumarinylmethyl cation and a leaving group anion[14]. This photolysis, long applied to controlled drug release[15,16], neurotransmitter uncaging[17], and intracellular pH manipulation[18] is redeployed to address packaging recyclability.

Our adhesive adopts a triblock architecture: two identical, non-polar outer blocks confer affinity with polyethylene, while the central polar block incorporates coumarin units and hydrogen-bond acceptors compatible with

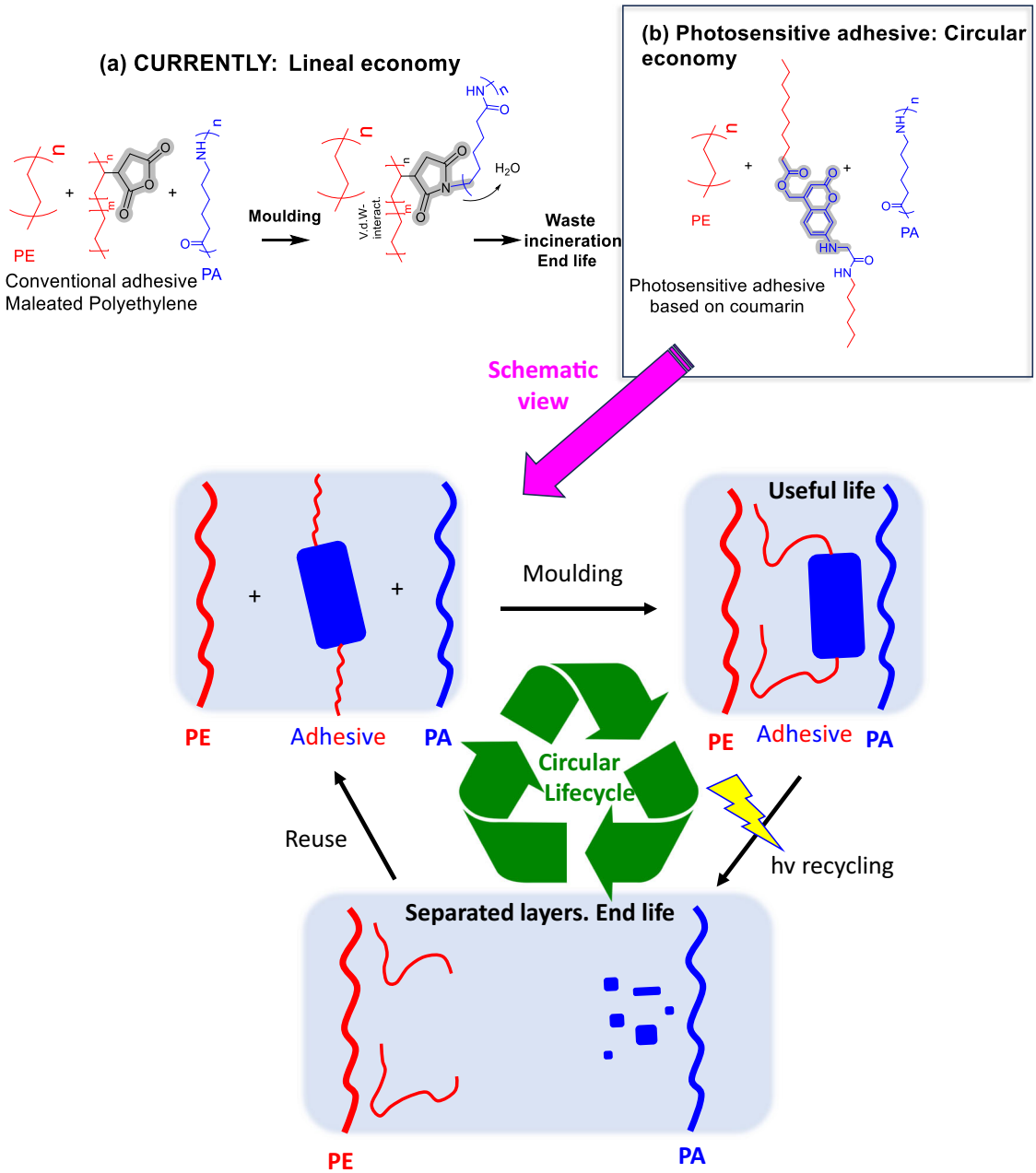


**Fig. 1 | Structural comparison between conventional and photosensitive PE–adh–PA adhesive systems. a** Conventional fabrication of non-reversible PE–adh–PA trilayer systems, where the olefinic domain of the adhesive forms secondary van der Waals interactions with the polyethylene (PE), while the maleic anhydride graft enables covalent bonding via condensation with the amide group of polyamide (PA). **b** Proposed photosensitive adhesive based on a triblock copolymer containing a coumarin unit. The adhesive establishes strong secondary interactions with PE and PA during its service life due to the structural similarity of the external blocks. Upon ultraviolet (UV).

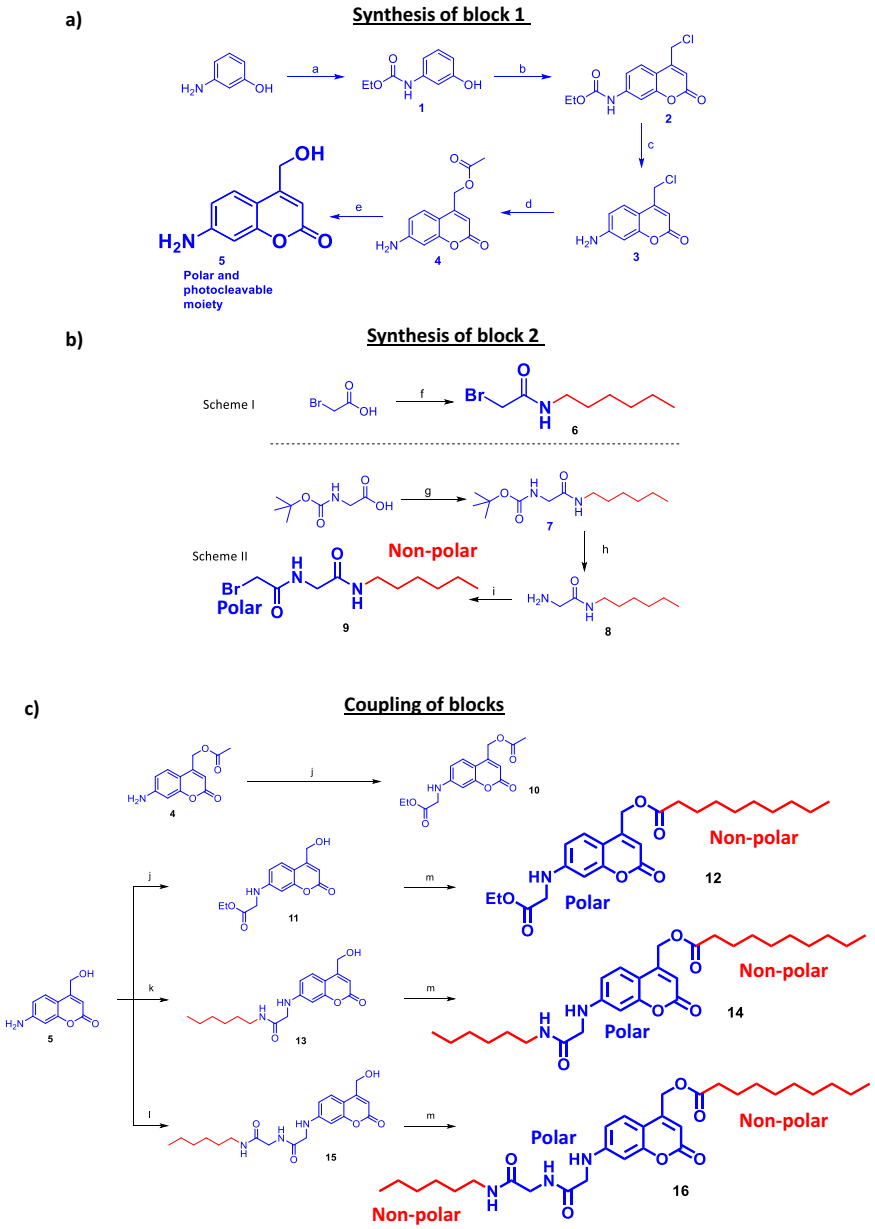


**Fig. 2 | Stepwise synthesis of the coumarin-based triblock adhesive components. a** Synthetic sequence for the preparation of 7-Amino-4-(hydroxymethyl)-2*H*-l-benzopyran-2-one. a) $ClCO_2Et$, AcOEt, Reflux, 50 min. b) Ethyl 2-chloroacetoacetate, $H_2SO_4$ (80%, aq), r.t., 4 h. c.1) $H_2SO_4$:AcOH (1:1), 125 °C, 2 h. c.2) ice, NaOH (3 M) until pH = 9. d) KOAc, $(n\text{-}Bu)_4NBr$ (cat.), DMF, 50 °C, 15 min; then r.t., 16 h. e) $K_2CO_3$, MeOH, r.t., 40 min. **b** Synthetic procedures for the preparation of polar-nonpolar block. f) N-hydroxysuccinimide, DCC, hexylamine, r.t. 16 h. g) N-hydroxysuccinimide, DCC, hexylamine, r.t. 16 h. h.1) HCl (4 M in Dioxane). h.2) $Na_2CO_3$ (aq.) until pH > 7. i) bromoacetic acid, *N*-hydroxysuccinimide, DCC, r.t. 16 h. **c** Synthesis of photosensitive coumarin derivatives. j) Ethyl bromoacetate (10 eq.), Et(i-Pr)2N (5 eq.), NaI (cat), DMF, $N_2$ atm., r.t., 16 h. k) Compound 6 (1.5 eq.), $Et(i\text{-}Pr)_2N$ (5 eq.), NaI (cat), DMF, $N_2$ atm., r.t., 16 h. l) Compound 9 (1.5 eq.), Et(i-Pr)2N (5 eq.), NaI (cat), DMF, $N_2$ atm., r.t., 16 h. m) Decanoyl chloride (1.3 eq.), $Et_3N$ (1.3 eq.), DMF:THF, $N_2$ atm., r.t., 16 h.

polyamide (See Fig. 1b). Unlike prior coumarin systems that exploit reversible dimerisation within crosslinked matrices, we engineer irreversible photofragmentation into a non-reversible, melt-processable thermoplastic tie. This preserves full compatibility with extrusion-lamination and thermocompression, requires no modification of the PE or PA substrates, and eliminates solvents or high mechanical energy during delamination. During service, the material behaves as a conventional tie layer, yet after exposure to light at 365 nm the coumarin domains fragment, the macromolecule disintegrates and the laminate delaminates cleanly—no solvent, no mechanical force, no residue. The terminal blocks are modular, enabling straightforward re-engineering towards other substrate chemistries (e.g., polyesters) while retaining the same light-addressable disassembly principle.

Crucially, this strategy differs from previous coumarin-based systems, which rely on photoreversible crosslinks within thermoset networks for self-healing coatings[19], dental cements or high-resolution patterning[20]. By embedding photolabile motifs in a non-reversible, melt-processable thermoplastic, we target the specific industrial challenge of multilayer packaging. In the pages that follow we detail the synthesis and physicochemical characterisation of this triblock adhesive, demonstrate its integration into PE–adhesive–PA laminates, quantify performance and light-triggered delamination, and present a preliminary life cycle assessment showing the potential environmental gains of the concept. Together, these results lay the groundwork for scalable, light-addressable recycling solutions in next-generation food packaging.

The photocleavable thermoplastic adhesive was prepared through a three-step modular strategy that assembles a low-molar-mass A–B functional architecture: an apolar, polyethylene-affine domain covalently linked to a polar, UV-labile domain based on a coumarin unit with amine/polar functionality. Although the synthetic route is built from three chemical modules (coumarin + PE-like chain + PA-like chain), in practice the coumarin plus amine/polar segment behave as a single PA-affine domain, while the terminal olefinic chain provides PE affinity. This construct compatibilises PE/PA during service and, upon 365 nm irradiation, undergoes selective loss of cohesion, enabling clean, residue-free delamination. (See Fig. 2a–c, for more details, refer to the Methods Section and the Supplementary Figs. 1.1–1.11).

## Results and discussion

### Challenges encountered during synthesis

Although the adhesive design was conceptually straightforward, its synthesis posed several challenges requiring careful optimisation of reaction conditions. A major difficulty occurred in the final step of preparing the coumarin moiety (Product 5, Fig. 2a). Following the conditions of Cürten et al.[21] led to low yields due to product degradation from prolonged reaction times, causing cleavage of the coumarin lactone ring. Reducing the reaction time to 40 minutes and isolating the solid by filtration significantly improved the yield and eliminated the need for methanol purification.

Regarding photochemical activity, two key structural features were critical. First, a hydroxymethyl group at position 4 of the coumarin core was essential for efficient photocleavage of ester-type bonds; replacing it with a carboxylic acid suppressed photoreactivity under identical conditions, underscoring the importance of this substituent[22]. Second, introducing an amide at the coumarin's amine group also inhibited photodegradation, and promoted dimerization. This was attributed to the electron-withdrawing nature of the amide, which reduced the electron density of the coumarin core. It was hypothesised that an aliphatic amine, as an electron donor, could enhance reactivity by restoring electron density.

Coupling the coumarin core with side chains also proved more complex than anticipated. Initial use of $K_2CO_3$ in the nucleophilic substitution reaction led to undesired ring-opening via ester hydrolysis, compromising photoactivity. Replacing $K_2CO_3$ with N,N-diisopropylethylamine, a milder non-nucleophilic base, prevented hydrolysis and improved reaction selectivity. Additionally, alkyl halides with extended methylene linkers failed due to the low nucleophilicity of aniline. This was resolved using bromoacetic acid derivatives with catalytic NaI, which enabled efficient substitution via enhanced α-carbon electrophilicity.

Achieving compatibility between side chains and both polar and nonpolar polymer matrices also required precise control over chain polarity and reactivity. During the synthesis of block 2, difficulties arose in amide bond formation. Using DCC alone generated cyclohexylurea byproducts that were difficult to remove, particularly for poorly soluble analogues. Adopting literature protocols[23] with *N*-hydroxysuccinimide as a coactivator allowed pre-filtration of urea byproducts, simplifying the isolation of block 2. Additionally, the aqueous solubility of amine 8 required water removal via rotary evaporation, followed by solid–liquid extraction using ethyl acetate.

### Photocleavage efficiency and mechanism

Once the coumarin models **12, 14** and **16** were synthesised. To investigate their photochemical behaviour under UV-light, samples were directly prepared as solutions in deuterated dimethylsulphoxide (DMSO-$d_6$). This strategy enabled the acquisition of $^1$H-NMR spectra both before and after UV irradiation. The objective was to monitor structural changes and to detect any photolytic products generated upon exposure to UV light (Fig. 3a).

$^1$H-NMR spectra of solutions of models **12, 14** and **16** were acquired and then these solutions were irradiated in the homemade photoreactor depicted in SI2 (See Supplementary Fig. 2.1) for 17 h at room temperature (approx. 20 °C). After this period, 1H-NMR spectra were recorded again.

In Fig. 3b, $^1$H NMR spectra of model **14** (DMSO-d6) before and after 365 nm irradiation are shown. Before irradiation, the diagnostic aromatic resonances of the coumarin core at $\delta \approx 6.2–7.9$ ppm (blue box) are clearly visible. After irradiation, these signals vanish, consistent with photolytic cleavage of the coumarin unit. By contrast, the aliphatic region ($\delta \approx 0.8–2.5$ ppm; red box) is preserved, including the α-methylene to the ester carbonyl, which shifts from $\delta \approx 2.40$ to ≈2.15 ppm, evidencing a changed electronic environment upon cleavage. Together, the loss of the coumarin aromatic manifold and the retention/shift of the aliphatic signatures provide direct NMR evidence for light-triggered fragmentation of model **14**.

In parallel experiments, irradiation at 254 nm resulted in significantly slower degradation, suggesting that irradiation at longer wavelengths (red-shifted) could potentially accelerate the photodegradation process. However, further experiments would be required to confirm this hypothesis. In contrast, the signals attributed to the aliphatic side chains (pink), including those of the decanoyl fragment, remain largely unaltered, suggesting that the structural integrity of the non-chromophoric regions is preserved. Notably, the methylene proton signal (2.40 ppm) located in α position to the ester carbonyl in the decanoyl chain undergoes an upfield shift to 2.15 ppm after irradiation, consistent with a change in its electronic environment resulting from the photolytic transformation. This observation supports the selective and efficient cleavage of the coumarin core while maintaining the side chain framework intact.

Upon exposure to UV irradiation, the coumarin moiety undergoes a photochemical transformation that results in the complete cleavage of its aromatic core (see Fig. 3c). In previous studies, the mechanism of cleavage between the carbonyl group in the ester and the hydroxymethylene group in (Coumarin-4-yl) methyl esters has been studied, and several proposals have been made[24]. This process is initiated by the absorption of UV light, which promotes the molecule to an excited electronic state. From this state, several reaction pathways may ensue, including intramolecular rearrangements, homolytic bond cleavage, or photooxidative processes, depending on the substituents and the surrounding environment[25]. In the present case, the disappearance of the aromatic signals in the NMR spectrum suggests a breakdown of the conjugated system, indicating that the coumarin core does not simply undergo bond scission at a specific position, but rather a more extensive decomposition[26]. To further demonstrate this, GC–MS (EI) analysis of the irradiated model 12 solution (SI2, Supplementary Figs. 2.2 and 2.3) revealed two main low-molecular-weight fragments at $m/z = 117$ and $m/z = 101$, corresponding to ethyl methylglycinate and ethyl 2-iminoacetate, respectively. These results indicate that UV exposure induces complete cleavage of the coumarin core, releasing small amine-derived fragments and likely forming decanoic acid as the complementary product —although the latter was not detected due to its polarity and retention on the GC column. Complementarily, the irradiated model 14 sample was analyzed by direct insertion mass spectrometry (ESI ±) and compared with its non-irradiated counterpart. The resulting mass spectra (See section SI2, Supplementary Figs. 2.4 and 2.5) are entirely different. In the non-irradiated sample spectrum, the exact mass peak corresponding to the intact coumarin-based structure is clearly observed. In addition, under the ESI conditions employed, a dominant signal was consistently observed at $m/z \approx 145$, which corresponds to the protonated coumarin fragment. This feature is characteristic of in-source fragmentation of coumarin derivatives, particularly when moderate to high cone voltages is applied. On the other hand, after irradiation, no recognizable fragments were detected, not even the coumarin fragment, confirming extensive molecular breakdown. Taken together, these findings corroborate that the coumarin linker undergoes complete photochemical fragmentation into volatile or low-mass residues, consistent with the NMR evidence of aromatic loss and explaining the efficient, residue-free delamination observed in the multilayer films. This behaviour has been previously investigated in the literature[26], where mechanistic studies have provided insights into the factors governing coumarin photostability and degradation pathways. The formation of such small fragments precludes, at least in a straightforward manner, the reformation of the original coumarin moiety; however, it may also offer the advantage of producing very pure layers of the remaining material, effectively recovering the underlying components prior to adhesive application.

Initially, we expected cleavage of the labile ester bond, as reported in many examples in the literature for similar structures[22]. However, instead of simple ester bond scission, the entire coumarin moiety undergoes photochemical cleavage, generating very small fragments. This precludes, at least in a straightforward manner, the reformation of the original coumarin unit and, consequently, the rebounding of the multilayer. On the other hand, these results are advantageous for our purpose, as complete photocleavage of the molecule enables the recovery of clean, residue-free polymeric layers, minimizing post-treatment and facilitating subsequent recycling of the materials.

Full fragmentation ensures that the photoreactive moiety breaks down into unidentified low molecular weight byproducts, which are more easily

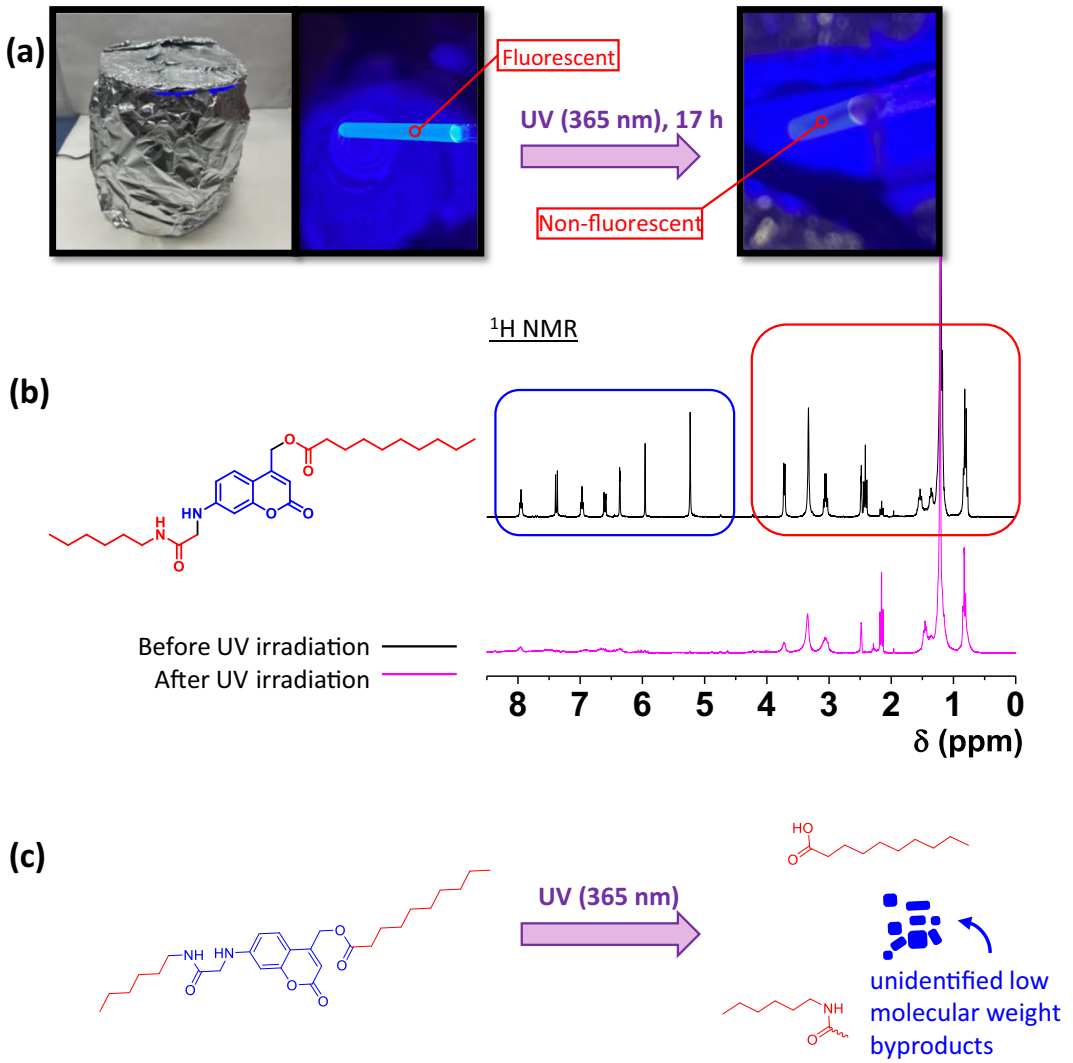


**Fig. 3 | Photocleavage behaviour of adhesive 14 under UV irradiation.** **a** Homemade photoreactor containing a solution of compound 14, before and after 17 hours of irradiation with 365 nm light. **b** $^1$H NMR spectra of coumarin model 14 before and after UV light-irradiation (365 nm, 17 h). **c** Proposed photochemical decomposition of model 14.

volatilized or removed from polymeric materials during multilayer separation processes. Another interesting point is the fact that the photocleavage process requires approximately 17 hours to complete, which means an advantage for its intended application in food packaging. This extended reaction time indicates slow photoreactivity under ambient conditions, providing the necessary stability during storage, transportation and display in supermarkets. If the system were more reactive, exposure to sunlight or antimicrobial UV lamps commonly used in stores could prematurely trigger the decomposition of the adhesive, compromising package integrity. This way, the material could remain intact during its functional lifetime.

### Performance and recycling assessment in multilayer packaging

Before assessing the adhesive's performance in multilayer film recyclability, the thermal stability of the individual components—polyethylene (PE), polyamide (PA), and the coumarin-based adhesives—was investigated. Differential scanning calorimetry (DSC) confirmed typical melting transitions for PE ( ~ 130 °C) and PA ( ~ 200 °C), supporting the use of 200 °C as the processing temperature. Among the synthesised adhesives, compound **14** exhibited the highest thermal stability, followed by compounds **12** and **10** (see Supplementary Fig. 3.1). This trend is attributed to structural differences: compound **10** contains thermally labile ester bonds, while compounds **12** and **14** incorporate more thermally resistant amide linkages. The superior stability of compound **14** is further supported by its long alkyl chains (hexyl and decanoate), which enhance dispersive interactions and lack oxygenated side groups, unlike compounds **10** and **12**. Moreover, nitrogen-linked coumarins (as in **14**) offer greater thermal resistance than their oxygen-linked counterparts. These findings justified the use of 220 °C for T-peel sample preparation (see Supplementary Fig. 3.2), ensuring full polymer melting without compromising adhesive integrity.

Figure 4 summarises the mechanical performance of the multilayer specimens. In the non-irradiated state, only the commercial adhesive (PE-g-MA) displayed a classical peel curve (Fig. 4a), with a maximum force of 115.8 N and an average of 86.9 N. The experimental adhesives exhibited distinct failure behaviours: compound **14** showed a markedly higher peak force (201.4 N; ~74% increase) with substrate failure (the joint could not be separated), whereas compounds **10** and **12** formed weak bonds indicative of adhesive failure. SEM images of the interfacial regions corroborated these observations.

Figure 4b classifies the failure modes: adhesive **14** induced substrate failure (b.1), the commercial adhesive produced cohesive failure (b.2), and adhesives 10 and 12 led to interfacial (adhesive) failure (b.3). The poor performance of adhesive **10** is attributable to the absence of functional groups compatible with either PE or PA. Despite bearing a polar substituent, adhesive **12** also failed to provide adequate bonding, likely due to insufficient

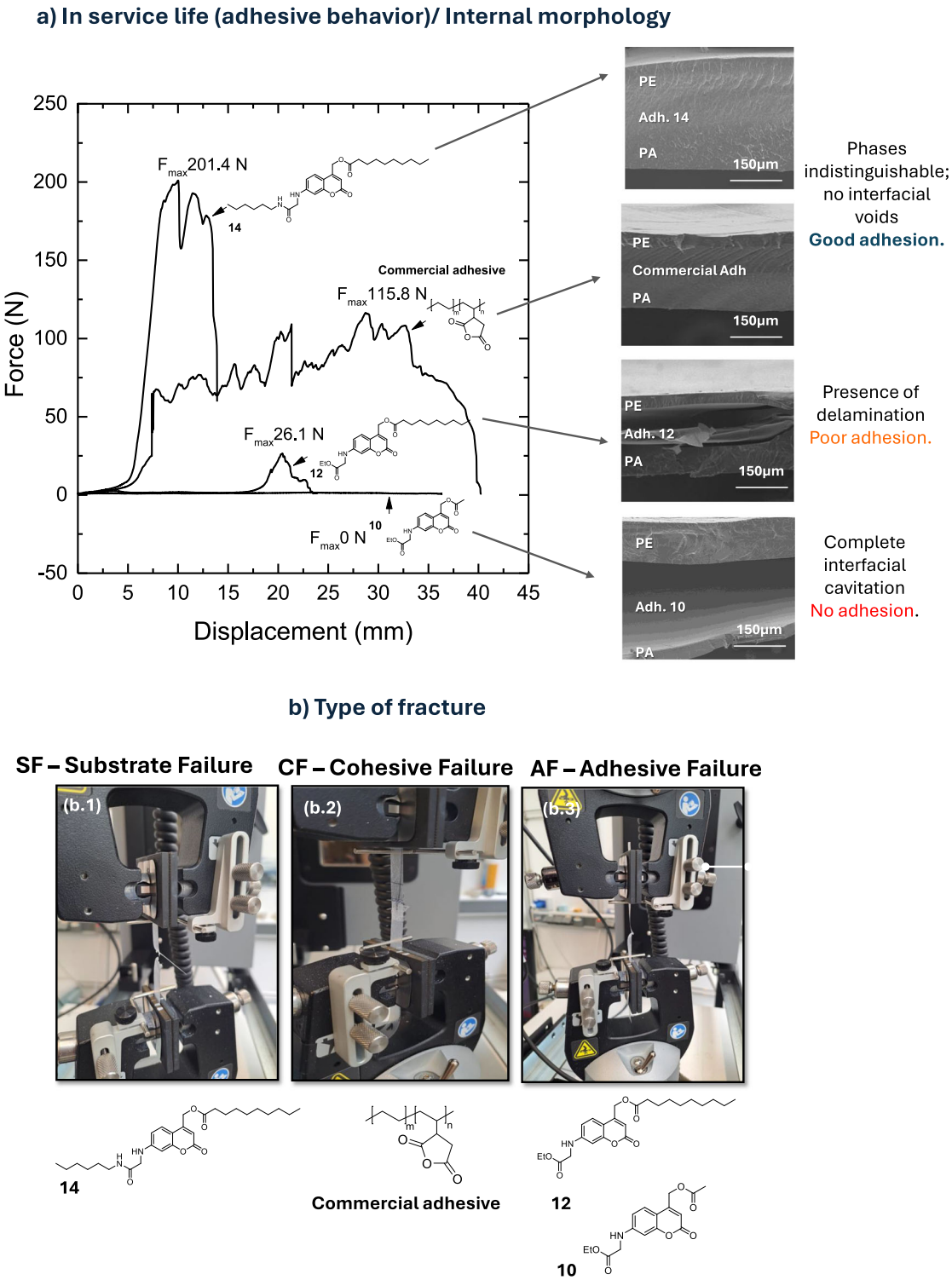


**Fig. 4 | Adhesive performance and failure modes of multilayer films before UV exposure. a** Force–displacement curves from T-peel tests of multilayer films bonded with different non-irradiated adhesives, along with SEM images of their interfacial regions. **b** Failure modes recorded after peel testing, classified by the type of adhesive used.

compatibilisation. SEM revealed large interfacial voids ( > 150 µm), confirming poor adhesion in these two systems.

By contrast, adhesive **14** achieved strong bonding owing to its dual compatibility: the decanoate and hexyl chains enhance interactions with PE, while the amide facilitates hydrogen bonding with PA. The commercial PE-g-MA system exhibited cohesive failure, consistent with maleic anhydride grafts bonding to PA[27] and compatibility imparted by the PE backbone.

Recyclability performance is shown in Fig. 5. After 72 h of UV exposure (see experimental setup in Supplementary Fig. 3.3), the commercial adhesive showed no change in bonding (its peel energy remains essentially invariant; Supplementary Table 3.1), indicating resistance to photodegradation and limited recyclability (Fig. 5a). In contrast, adhesive 14 exhibited a progressive loss of adhesion under UV (Fig. 5b): substrate failure transitioned to cohesive failure after 17 h and to near-complete delamination after 72 h, as confirmed by SEM micrographs showing microcavity formation and adhesive

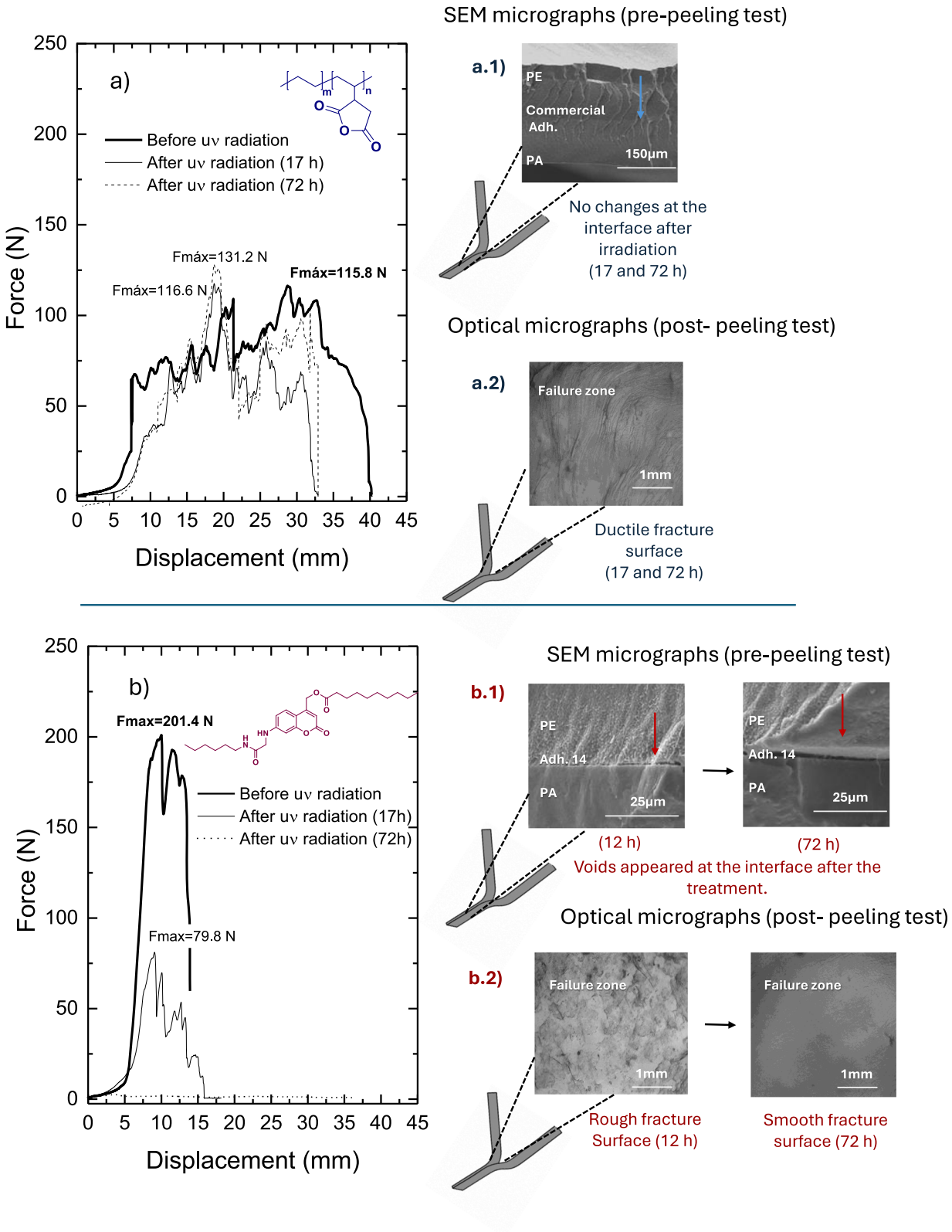


**Fig. 5 | Recycling performance of commercial and photosensitive adhesives under UV exposure. a** Force–displacement curves from T-peel tests of the commercial adhesive before and after UV exposure (17 h and 72 h). **b** Force–displacement curves of adhesive **14** under the same UV exposure conditions. (a.1) and (b.1) SEM images of the adhesive interfaces before and after irradiation. (a.2) and (b.2) Optical micrographs of failure zones following the T-peel test.

degradation. Consistently, Supplementary Table 3.1 shows that both maximum forces and peel energies for adhesive 14 decrease rapidly to zero with irradiation time. This behaviour aligns with previous reports on coumarin-based thermoset systems undergoing UV-induced bond scission[28].

Optical microscopy supported these findings. The commercial adhesive showed plastic deformation, whereas adhesive **14** revealed surface roughness after 17 h and complete smoothing after 72 h, indicating adhesive loss. FTIR analysis of the separated layers (see Supplementary

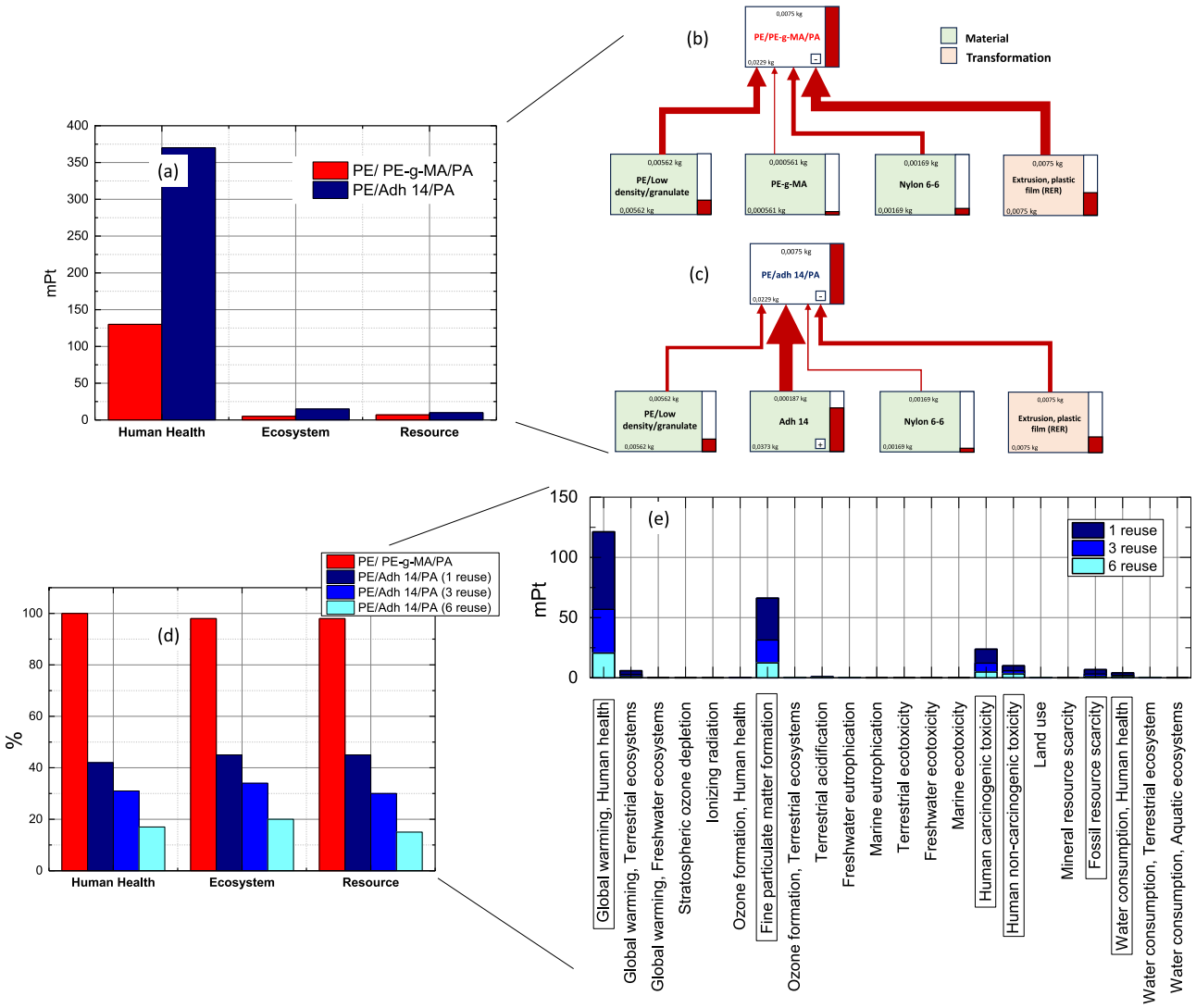


**Fig. 6 | Life cycle assessment of commercial versus photosensitive adhesive systems for multilayer packaging. a** Normalised environmental impact per functional unit (1 kg of PE–adhesive–PA film) in the categories of human health, ecosystem quality, and resource use, comparing a commercial maleic anhydride-grafted PE adhesive and the photosensitive adhesive 14 (laboratory-scale synthesis). **b** Life cycle inventory (LCI) contribution analysis for the commercial multilayer system, highlighting the dominant impact of PE production and extrusion-lamination processes. **c** LCI contribution analysis for the photosensitive multilayer system, showing the major contribution from laboratory-scale synthesis of adhesive 14. **d** Environmental impact normalised to the commercial single-use reference scenario, for the photosensitive multilayer system assuming industrial-scale adhesive production and 1 to 6 reuse cycles. **e** Breakdown of impact categories most affected in the photosensitive system, identifying hotspots such as global warming potential, fine particulate matter formation, carcinogenic emissions, water use, and fossil resource scarcity.

Fig. 4.1) confirmed minimal contamination: PE showed no adhesive signals, and PA exhibited only minor residual bands (1000–1500 $cm^{-1}$), which largely disappeared after ethanol washing. These results confirm that the proposed adhesive allows clean delamination and reuse of both polymer layers, significantly enhancing multilayer packaging recyclability.

Finally, it is important to note that the specimens were consistently stored under ambient laboratory light and temperature from fabrication to testing ( ≥ 7 days). Under these conditions, no detectable changes in peel behaviour (force–displacement profile and failure mode) were observed relative to samples stored protected from light. Given that delamination in our set-up requires targeted 365 nm irradiation and prolonged exposure, the adhesive remains stable under typical handling. As the intended application concerns short-shelf-life food packaging, stability over several days appears sufficient; nevertheless, comprehensive environmental ageing tests (controlled UV dose and thermal/hygrometric stress) will be addressed in future work.

## Environmental impact assessment through life cycle analysis

Figure 6a presents the environmental impact assessment associated with the production of a functional unit (one multilayer food packaging film), comparing two adhesive systems: a conventional single-use commercial adhesive (PE-g-MA) and the newly developed photosensitive adhesive 14. Three key areas of protection were considered, following the ReCiPe and LC-IMPACT methodologies: human health, ecosystem quality, and resource availability[29]. At first glance, it becomes evident that, in its current laboratory-scale development, the use of adhesive 14 may result in up to threefold higher environmental impact across all categories compared to the commercial alternative, with the most pronounced effect observed in the *human health* category. This increase is primarily attributed to the use of organic solvents and hazardous reagents during the multi-step synthesis of the photosensitive adhesive. According to standard life cycle impact assessment (LCIA) methodologies, the *human health* impact category aggregates the burden of toxic emissions into air, water, and soil, as well as exposure to carcinogenic and non-carcinogenic substances, photochemical

ozone formation, and particulate matter formation. Laboratory-scale synthesis often lacks solvent recovery systems and energy-efficient protocols, leading to higher emissions per functional unit. In contrast, the commercial maleated polyethylene adhesive benefits from more mature, large-scale manufacturing processes with optimised resource efficiency and emissions control, thereby exhibiting significantly lower impact in this category.

Analysis of the material and process flows involved in both systems (Fig. 6b, c) reveals that, for the conventional multilayer film, the main contributors to the environmental burden are the production of polyethylene and the extrusion and lamination steps. In contrast, in the photosensitive system, these factors play a minor role when compared to the dominant impact associated with the laboratory-scale production of adhesive 14. The complete process flow designed to evaluate the environmental impact of adhesive 14 synthesis—up to the formation of intermediate compound 5—is detailed in Supplementary Fig. 5.

This finding highlights the critical importance of scaling up and optimising the production of the photosensitive adhesive to achieve environmental viability. Similar trends have been reported in the literature; the environmental advantages of innovative materials are significantly offset by the burdens incurred during early development stages[30].

To assess the potential benefit of industrially optimised manufacturing, scenarios were modelled where adhesive 14 was produced at scale and used in multilayer films that allow for effective separation and reuse of polymer layers for at least six cycles—considered the upper threshold for mechanical recycling of polyamide without significant deterioration in properties. Under these assumptions, the results shown in Fig. 6d indicate a substantial improvement in environmental performance. Compared to the baseline single-use commercial system, environmental impact reductions of approximately 60% can be achieved after just one reuse cycle, increasing to 70% and 80% after three and six cycles, respectively.

These results provide strong justification for continued investment in the development and scale-up of photosensitive adhesives. Furthermore, Fig. 6e identifies the most influential impact categories where improvements would have the greatest benefit: global warming potential associated with energy use, fine particulate matter formation, carcinogenic emissions, water consumption, and fossil resource scarcity.

In conclusion, this study demonstrates that although photosensitive adhesives currently entail a considerable environmental burden during early-stage synthesis, their successful implementation at the industrial scale—together with validated recyclability in multilayer PE–PA structures—offers significant environmental advantages. The adhesive model presented here serves as a proof of concept for a new class of thermoplastic materials that combine photo-triggered delamination with standard processability. Importantly, the modular triblock design opens avenues for the rational development of alternative block copolymers with tailored terminal segments, enabling compatibility with a broader range of polymers such as polyesters. This platform thus provides a versatile foundation for engineering next-generation adhesives for applications in the circular economy in complex multilayer packaging systems.

## Methods

### Materials

All common reagents and solvents were obtained from commercial suppliers and used without any further purification. Hexane and EtOAc for flash column chromatography were purchased as extra pure-grade reagents and used as received. Commercial reagents: 3-aminophenol (Sigma Aldrich, 99%), ethyl chloroformate (Alfa Aesar, 97%), ethyl 2-chloroacetoacetate (Sigma Aldrich, 95%), sulphuric acid ($H_2SO_4$, VWR Chemicals, 95%), acetic acid (AcOH, Merck, >99%), potassium acetate (Thermo Scientific, 99%), tetra(*n*-butyl)ammonium bromide (Alfa Aesar, 98%), *N,N*-dimethylformamide (DMF, Merck, >99%), sodium hydroxide (NaOH, VWR Chemicals, 99%), hydrochloric acid (HCl, VWR Chemicals, 37%), potassium carbonate anhydrous ($K_2CO_3$ (anh.), Alfa Aesar, 99%), methanol (MeOH, VWR Chemicals, >99%), bromoacetic acid (TCI, 98%), *N,N*'-dicyclohexylcarbodiimide (DCC, Alfa Aesar, 99%), 1-hexylamine (TCI, 99%), *N*-hydroxysuccinimide (Alfa Aesar, 98%), sodium carbonate ($Na_2CO_3$, Sigma Aldrich, >99%), ethyl bromoacetate (Alfa Aesar, 98%), ethyldiisopropylamine (Merck, 98%), sodium iodide (NaI, Scharlau, 99%), decanoyl chloride (TCI, 98%), tetrahydrofuran anhydrous (THF (anh.), VWR Chemicals, >99%), deuterated methanol (MeOD-$d_4$, VWR Chemicals, 99.8%), deuterated dimethylsulphoxide (DMSO-$d_6$, VWR Chemicals, 99.8%), *N*-(tert-butoxycarbonyl)glycine, (Boc-Gly-OH, Sigma Aldrich, 99%), dioxane (VWR Chemicals, >99%). All reactions involving air-sensitive compounds were carried out under a nitrogen atmosphere ($N_2$, 99.99%). All glassware was oven-dried (120 °C), evacuated and purged with nitrogen.

To evaluate the performance of the designed adhesive models, a trilayer structure composed of polyethylene (PE)—adhesive—polyamide (PA) was fabricated. The PE used was HDPE 4910, supplied by REPSOL; the PA was PA5033B, supplied by UBE; and the commercial thermoplastic adhesive employed was a maleic anhydride-grafted polyethylene (PE-g-MA), FUSABOND E226, supplied by Dow Chemical.

### Synthesis of photocleavable model thermoplastic adhesive

The synthesis of the photocleavable model adhesive was carried out in three clearly defined stages: (i) synthesis of block 1 (central polar block based on a coumarin moiety, compatible with PA), (ii) synthesis of block 2 (terminal polar and nonpolar block, dual compatibility), and (iii) selection of block 3 (terminal nonpolar block, compatible with PE) and coupling to yield the final photocleavable model adhesive.

**(i) Synthesis of block 1 (central polar block based on a coumarin moiety, compatible with PA).** The synthesis was previously reported by other authors in five different reaction steps[21]. In the present study, these steps were slightly modified and adapted. Detailed information regarding the synthesis and characterisation of all compounds can be found in the Supplementary Information SI1.

**(ii) Synthesis of block 2 (terminal polar and nonpolar block, dual compatibility).** The synthesis of block 2 was carried out by amide bond formation reactions employing a combination of DCC and *N*-hydroxysuccinimide as the coupling agent. In this sense, amide 6 was synthesised by coupling bromoacetic acid and hexylamine. On the other hand, for the preparation of block 2 with two amide groups, Boc-glycine was used as the starting material. An amide bond formation reaction was performed with hexylamine, obtaining carbamate 7. Then, Boc-protecting group on the amine was removed by aqueous acid treatment to obtain amine 8, which was subsequently employed in the amide bond formation with bromoacetic acid. Detailed information regarding the synthesis and characterisation of all compounds can be found in the Supplementary Information SI1.

**(iii) Selection of block 3 (terminal nonpolar block, compatible with PE) and coupling to yield the final photocleavable model adhesive.** Decanoyl chloride was selected as block 3 and was commercially acquired. Once blocks 1 and 2 were synthesised, a nucleophilic substitution reaction was carried out between the amino group of block 1 and the alkyl halide of block 2. Finally, block 3 was introduced at the hydroxymethyl group located at position 3 of the coumarin core (block 1) via a substitution reaction. Detailed information on the synthesis and characterisation is provided in the Supplementary Information SI1.

### Instrumentation and characterisation of photocleavable model thermoplastic adhesive

Thin-layer chromatography (TLC) was performed on aluminium-backed plates coated with silica gel 60 with F254 indicator; the chromatograms were visualised under ultraviolet light and/or by staining with a Ce/Mo reagent and subsequent heating. $R_f$ values are reported on silica gel. Flash column chromatography was carried out on silica gel 60, 230–240 mesh. $^1H$ and $^{13}C$

NMR spectra were recorded in deuterated dimethylsulphoxide (DMSO-$d_6$) using a Bruker Avance III HD or a Varian Mercury-Plus spectrometer operating at 300 and 75 MHz, respectively. High-resolution mass spectra (HRMS) were obtained on a Micromass Autospec spectrometer using EI at 70 eV or on an Agilent 6545 Q-TOF mass spectrometer using electrospray ionization (ESI).

Melting points of compounds 10–16 were measured on a Gallenkamp apparatus using open capillary tubes and are uncorrected. UV irradiation tests were performed in a homemade equipment in which a mesh structure, serving as the support, was wrapped in aluminium foil to enhance reflectivity. The interior of the device was lined with a stripe of ultraviolet (368 nm) LED lights to provide the necessary irradiation for the reaction (more information in Supplementary Information, SI2- Supplementary Fig. 2.1).

### Fabrication and characterisation of multilayer films

Individual polymer films of polyethylene (PE), polyamide (PA), and the selected adhesive models were first prepared by compression moulding using a hot-plate press. Prior to processing, polyamide (PA) granules were dried in a convection oven at 80 °C for 24 h to eliminate residual moisture. Each polymer was processed separately by placing the pellets between two PTFE-coated stainless steel plates and applying a standardised thermal cycle: heating to the polymer-specific melting temperature (230 °C for PA, 190 °C for PE, and 180 °C for PE-g-MA), followed by a pre-heating stage without pressure to allow for the release of volatiles. Subsequently, a pressure of 15,000 tonnes of force was applied for 2 min to ensure film consolidation. The mould was then rapidly cooled to 25 °C using a cold press under the same pressure for an additional 5 minutes. The resulting films exhibited a uniform thickness of approximately 0.1 cm.

Multilayer PE–adh–PA structures were then assembled by stacking the individual films and repeating the compression moulding cycle under the same thermal and pressure conditions to ensure adequate interfacial adhesion. Peel test specimens were prepared from these multilayer assemblies following the methodology detailed in Supplementary Fig. 3.2. The composition of the multilayer specimens used for peel testing were: PE-Adh**10**-PA, PE-Adh**12**-PA, PE-Adh**14**-PA and PE-(PE-g-MA)-PA. Adh**16** was excluded from this stage, as it represents an alternative synthetic route but possesses the same functional composition as Model **14**.

Thermal transitions—including the melting temperatures of the neat polymers and the decomposition temperatures of the adhesive compounds, which are critical for designing the lamination process of the multilayer films—were determined by differential scanning calorimetry (DSC, Mettler Toledo DSC 821e). For PE and PE-g-MA, a heating scan was conducted from –40 °C to 200 °C at a rate of 10 °C/min under nitrogen atmosphere. In the case of PA, the thermal scan was carried out from 0 °C to 300 °C at the same heating rate and inert conditions. The melting temperature was taken as the peak of the endothermic transition observed during the first heating run. For the adhesive additives, a heating scan from 20 to 300 °C was performed at 10 °C/min under an oxidative atmosphere. The decomposition temperature was defined as the onset temperature at which an exothermic peak corresponding to thermal degradation began to emerge (See Supplementary Fig. 3.1).

### Interfacial compatibility and phase-separation assessment

The adhesive performance of the multilayer films was assessed using T-peel tests in accordance with ASTM D903, a standard method for evaluating the peel resistance of bonded flexible assemblies. In this test, the bonded films were pulled apart in a 'T' configuration to determine the force required for separation, considering maximun peel force, average peel force and peel energy.(See Supplementary Fig. 3.2). To assess the quality of the interfacial adhesion, cross-sectional images of the multilayer structure were obtained using scanning electron microscopy (SEM), employing a FlexSEM 1000 VP-SEM (Hitachi High-Technologies). Samples were cryo-fractured in liquid nitrogen to preserve morphological features and then sputter-coated with a thin layer of gold to ensure conductivity prior to observation. Once interfacial adhesion quality was confirmed, the T-peel test was subsequently carried out using an Instron universal testing machine (Model 5500R60025) fitted with a 500 N load cell. Test specimens were prepared by cutting the laminated films into strips measuring 10 mm in width and 100 mm in length. Peeling was conducted at a constant crosshead speed of 50 mm/min under ambient laboratory conditions (50% relative humidity and 25 °C).

For each adhesive formulation, a minimum of five replicates was tested to ensure statistical relevance. The maximum peel force, average peel strength, and peel energy were recorded for each sample and compared to evaluate the adhesive efficacy of the different formulations.

To evaluate the photodegradability of the adhesive layer, the multilayer films were irradiated using a UV lamp (wavelength: 365 nm) with a custom-built setup described in Supplementary Fig. 3.3, for up to 72 h. Following irradiation, the quality of the interfacial bonding was re-examined by scanning electron microscopy (SEM), and T-peel tests were repeated under the exact same conditions as those applied to the non-irradiated reference samples. Fracture surfaces were further inspected by optical microscopy (DM2500 M, Leica). The presence of residual adhesive on the polymer surfaces was evaluated using attenuated total reflectance Fourier transform infrared spectroscopy (ATR-FTIR, Tensor 27, Bruker).

### Life cycle assessment summary

A comparative life cycle assessment (LCA) was carried out to evaluate the environmental performance of a photodetachable coumarin-based adhesive (compound **14**) compared with a conventional maleic anhydride-grafted polyethylene (PE-g-MA) adhesive. The study considered the full life cycle of a multilayer packaging structure and quantifies the potential environmental benefits associated with the adoption of photosensitive adhesive under scalable production and reuse conditions.

The functional unit selected for this analysis was the multilayer film used as the sealing lid of a standard rigid food tray (30 × 25 × 10 cm), with a total mass ranging between 7.5 and 9.0 g. The film consisted of a three-layer PE–adh–PA configuration, composed of 75 wt% polyethylene (PE), 22.5 wt % polyamide (PA), and 2.5 wt% adhesive, reflecting typical industrial layer thicknesses.

The system boundaries were defined using a truncated cradle-to-grave approach, comprising adhesive synthesis, multilayer film fabrication, use phase (including multiple reuse cycles), and end-of-life disposal. For compound **14**, laboratory-scale synthesis data were used to estimate energy consumption and emissions. In contrast, the commercial adhesive was modelled using life cycle inventory data available in the Ecoinvent database for maleated polyethylene. Although the application of adhesive **14** may involve different processing (e.g., application by spraying or gluing), such variations were considered negligible in terms of energy use and were not differentiated in the model.

The assessment focused on cumulative environmental impacts per functional unit over multiple reuse cycles. The UV-induced delamination enabled by adhesive 14 allows the separation and potential reuse of both polymer substrates. It was assumed that this delamination process is effective and repeatable in each cycle, based on experimental confirmation of adhesive photodegradation and clean interfacial separation. Additionally, the assumption that residual adhesive does not impair the recyclability of the polymers was supported by ATR-FTIR and TGA analysis, which revealed minimal contamination on the recovered PE and PA surfaces.

Regarding polymer durability, literature reports indicate that polyethylene can endure up to 40 extrusion cycles under mechanical recycling conditions before significant degradation occurs[31], while PA6 and PA66 maintain acceptable properties for approximately six cycles[32]. A sixquently, a six-cycle reuse threshold was selected for this LCA, providing a conservative yet realistic framework. For modelling recycling steps, standard twin-screw extrusion was assumed, and the energy input associated with UV delamination was calculated based on laboratory-scale exposure times and scaled to reflect plausible industrial operation.

The end-of-life scenario for both adhesive systems was assumed to be incineration, consistent with current disposal practices for non-recyclable

packaging. The LCA aimed to quantify the relative contribution of the adhesive synthesis process to the overall environmental impact and to validate the environmental viability of a light-responsive adhesive system under circular economy principles.

## Data availability

The data that support the findings of this study are available within the article and its Supplementary Information files.

Received: 25 June 2025; Accepted: 8 December 2025;
Published online: 24 December 2025

## References

1. Tamizhdurai, P. et al. A state-of-the-art review of multilayer packaging recycling: Challenges, alternatives, and outlook. *J. Clean. Prod.* **447**, 141403 (2024).
2. Plastics Europe Plastics – the Facts. https://plasticseurope.org/knowledge-hub/plastics-the-facts-2020 (2020).
3. Kaiser, K., Schmid, M. & Schlummer, M. Recycling of polymer-based multilayer packaging: A review. *Recycling* **3**, 1 (2017).
4. Soares, C. T. et al. Recycling of multi-material multilayer plastic packaging: Current trends and future scenarios. *Resour. Conserv Recycl* **176**, 105905 (2022).
5. De Feo, G., Ferrara, C. & Minichini, F. Comparison between the perceived and actual environmental sustainability of beverage packagings in glass, plastic, and aluminium. *J. Clean. Prod.* **333**, 130158 (2022).
6. Ketelsen, M., Janssen, M. & Hamm, U. Consumers' response to environmentally-friendly food packaging - A systematic review. *J. Clean. Prod.* **254**, 120123 (2020).
7. Dinte, E. & Sylvester, B. Adhesives: Applications and Recent Advances. in *Applied Adhesive Bonding in Science and Technology* (InTech), https://doi.org/10.5772/intechopen.71854 (2018).
8. Walker, T. W. et al. Recycling of multilayer plastic packaging materials by solvent-targeted recovery and precipitation. *Sci. Adv.* **6**, 1–9 (2020).
9. Pappa, G. et al. The selective dissolution/precipitation technique for polymer recycling: a pilot unit application. *Resour. Conserv Recycl* **34**, 33–44 (2001).
10. Li, T. et al. Progress in solvent-based recycling of polymers from multilayer packaging. *Polym. (Basel)* **16**, 1670 (2024).
11. Kaiser, K. M. A. Recycling of multilayer packaging using a reversible cross-linking adhesive. *J. Appl. Polym. Sci.* **137**, 1–12 (2020).
12. Guo, J., Hemmatpour, H., Aggarwal, L., Rudolf, P. & Bose, R. K. Healable and debondable poly(furfuryl methacrylate) thin film adhesive based on Diels–Alder networks. *ACS Appl Polym. Mater.* **7**, 889–900 (2025).
13. Salavagione, H. J. et al. Remotely triggered reversible bonds in adhesives for sustainable multi-layered packaging. *Sustain. Mater. Technol.* **36**, e00632 (2023).
14. Chatani, S., Kloxin, C. J. & Bowman, C. N. The power of light in polymer science: photochemical processes to manipulate polymer formation, structure, and properties. *Polym. Chem.* **5**, 2187–2201 (2014).
15. Rahimi, S., Khoee, S. & Ghandi, M. Development of photo and pH dual crosslinked coumarin-containing chitosan nanoparticles for controlled drug release. *Carbohydr. Polym.* **201**, 236–245 (2018).
16. de Gracia Lux, C. et al. Short soluble coumarin crosslinkers for light-controlled release of cells and proteins from hydrogels. *Biomacromolecules* **16**, 3286–3296 (2015).
17. Stefanello, T. F. et al. Coumarin-containing thermoresponsive hyaluronic acid-based nanogels as delivery systems for anticancer chemotherapy. *Nanoscale* **9**, 12150–12162 (2017).
18. Safavi-Mirmahalleh, S.-A., Golshan, M., Gheitarani, B., Salami Hosseini, M. & Salami-Kalajahi, M. A review on applications of coumarin and its derivatives in preparation of photo-responsive polymers. *Eur. Polym. J.* **198**, 112430 (2023).
19. Hughes, T., Simon, G. P. & Saito, K. Photocuring of 4-arm coumarin-functionalised monomers to form highly photoreversible crosslinked epoxy coatings. *Polym. Chem.* **10**, 2134–2142 (2019).
20. Chen, Q. et al. Photopolymerization of coumarin-containing reversible photoresponsive materials based on wavelength selectivity. *Ind. Eng. Chem. Res* **58**, 2970–2975 (2019).
21. Cürten, B., Kullmann, P. H. M., Bier, M. E., Kandler, K. & Schmidt, B. F. Synthesis, photophysical, photochemical and biological properties of caged GABA, 4-[[(2H-1-Benzopyran-2-one-7-amino-4-methoxy) carbonyl] amino] butanoic acid. *Photochem Photobio.* **81**, 641–648 (2005).
22. Klán, P. et al. Photoremovable protecting groups in chemistry and biology: Reaction mechanisms and efficacy. *Chem. Rev.* **113**, 119–191 (2013).
23. Datta, A., Quintavalla, S. M. & Groves, J. T. Kinetic selectivity in the N-alkylation of 2-pyridyl porphyrins: A facile approach to the ααββ scaffold. *J. Org. Chem.* **72**, 1818–1821 (2007).
24. Schmidt, R., Geissler, D., Hagen, V. & Bendig, J. Mechanism of photocleavage of (coumarin-4-yl)methyl esters. *J. Phys. Chem. A* **111**, 5768–5774 (2007).
25. Bryantseva, N. G., Tchaikovskaya, O. N., Kraiukhina, V. S., Gómez, M. & Gómez, J. L. Photodegradation of some furocoumarins in ethanol under UV irradiation. *Key Eng. Mater.* **683**, 402–405 (2016).
26. Yang, Q., Váňa, J. & Klán, P. The complex photochemistry of coumarin-3-carboxylic acid in acetonitrile and methanol. *Photochem. Photobiol. Sci.* **21**, 1481–1495 (2022).
27. Srinivasan, D. V., Aggarwal, A. & Idapalapati, S. Temperature-dependent peel performance of adhesively rebonded hybrid joints. *Int J. Adhes. Adhes.* **97**, 102474 (2020).
28. Andre, J. S. et al. Ultraviolet light-sensitive debonding layer for reducing adhesion of polymer adhesives for recycling. *J. Phys. Chem. C.* **126**, 18907–18917 (2022).
29. Verones, F. et al. LCIA framework and cross-cutting issues guidance within the UNEP-SETAC Life Cycle Initiative. *J. Clean. Prod.* **161**, 957–967 (2017).
30. Verones, F. et al. LC-IMPACT: A regionalized life cycle damage assessment method. *J. Ind. Ecol.* **24**, 1201–1219 (2020).
31. Jin, H., Gonzalez-Gutierrez, J., Oblak, P., Zupančič, B. & Emri, I. The effect of extensive mechanical recycling on the properties of low density polyethylene. *Polym. Degrad. Stab.* **97**, 2262–2272 (2012).
32. Ben Amor, I., Klinkova, O., Baklouti, M., Elleuch, R. & Tawfiq, I. Mechanical recycling and its effects on the physical and mechanical properties of polyamides. *Polym. (Basel)* **15**, 4561 (2023).

## Acknowledgements

We gratefully acknowledge financial support from the Spanish Ministry of Science and Innovation (Ministerio de Ciencia e Innovación, MCIN), the Spanish State Research Agency (Agencia Estatal de Investigación, AEI) and the European Union—NextGenerationEU, through the ECOLAYER project (TED2021-129419B-C21/C22) (J.C.M. and J.M.G.), and through grant PID2023-147301OB-I00 funded by MICIU/AEI/10.13039/501100011033 and by the European Regional Development Fund (FEDER/ERDF, EU) (J.M.G. and S.V.). They also acknowledge the Recovery and Resilience Mechanism Funds (NextGenerationEU and Castilla y León Funds) under the Complementary R&D&I Plans with the Autonomous Communities, Component 17—Investment 1 (M.A.R.P.). Financial support provided by the European Regional Development Fund (FEDER/ERDF) and the Regional Government of Castilla y León—Consejería de Educación, Junta de Castilla y León—under project BU025P23 is gratefully acknowledged. Author S. Vallejos acknowledges funding received through grant BG22/00086, funded by the Spanish Ministry of Universities (Ministerio de Universidades, Spain). Additionally, the authors thank the University of Valladolid for the Post-doctoral Contract awarded under the 2020 Call (K.C.N.C.). Finally, they

acknowledge the support of the Spanish State Research Agency (Agencia Estatal de Investigación, AEI) and the Spanish Ministry of Science and Innovation (Ministerio de Ciencia e Innovación, MCIN) for funding the Synergy Project CNS2023-144442 aimed at the consolidation of the research activity of K.C.N.C.

## Author contributions

C. S.: Validation, Investigation, Methodology, Writing—Original Draft. M. H.: Validation, Investigation, Methodology. M. T.: Methodology, Validation, Formal analysis, Investigation, Writing—Original Draft. M. A. R. P.: Resources, Funding acquisition. J. C. M.: Resources, Funding acquisition. J. M. G.: Conceptualization, Methodology, Supervision, Funding acquisition. S. V.: Conceptualization, Funding acquisition, Project administration, Methodology, Investigation, Writing–Original Draft, Writing—Review & Editing, Supervision. K. C. N. C.: Conceptualization, Funding acquisition, Project administration, Methodology, Investigation, Writing–Original Draft, Writing—Review & Editing, Supervision.

## Competing interests

The authors declare no competing interests.

## Additional information

**Supplementary information** The online version contains supplementary material available at https://doi.org/10.1038/s43246-025-01040-6.

**Correspondence** and requests for materials should be addressed to Saul Vallejos or Karina C. Núñez Carrero.

**Peer review information** *Communications Materials* thanks Luke Henderson, Bhagya Dharmasiri and the other, anonymous, reviewer(s) for their contribution to the peer review of this work. A peer review file is available.